Measurement of Radiated Power Using an InfraRed Imaging Video Bolometer System in the Upstream of GAMMA 10/PDX Divertor Simulation Plasma*)

Naoki SHIGEMATSU, Naomichi EZUMI, Kiyofumi MUKAI[1,2)], Takumi SETO, Takuma OKAMOTO, Kosuke TAKANASHI, Satoshi TAKAHASHI, Reina MIYAUCHI, Satoshi TOGO, Mafumi HIRATA, Junko KOHAGURA, Masayuki YOSHIKAWA, Ryutaro MINAMI, Yousuke NAKASHIMA and Mizuki SAKAMOTO

Plasma Research Center, University of Tsukuba, Tsukuba 305-8577, Japan
[1)]*National Institute for Fusion Science, Toki 509-5292, Japan*
[2)]*The Graduate University for Advanced Studies, SOKENDAI Toki 509-5292, Japan*

(Received 9 January 2023 / Accepted 26 March 2023)

Plasma radiation intensity distribution plays a crucial role in the energy balance and impurity transport during plasma detachment. An InfraRed imaging Video Bolometer (IRVB) is a radiation distribution measurement system, that uses an infrared camera to measure the temperature distribution on a thin foil caused by plasma radiation. Herein, an IRVB measurement system is installed in the west plug/barrier cell of the GAMMA 10/PDX, which is upstream of the divertor-simulated plasma. In the case of Ar injection, a clear difference is observed in the plasma radiation intensity depending on the incident gas pressure. However, during Ne injection, the difference in the plasma radiation intensity is not clear. Compared with the case of Ne, the radiation intensity is higher when Ar gas was injected.

Keywords: radiation, bolometer, IRVB, plasma detachment, divertor, D-module, GAMMA 10/PDX

DOI: 10.1585/pfr.18.2402031

1. Introduction

To realize fusion reactors, the heat load on divertor target plates must be reduced. One promising approach is detached plasma formation mediated by radiation cooling of the plasma caused by impurity gas puffing [1]. However, the spreading of the radiation region leads to the dilution of the core plasma. In addition, radiation loss is an important factor affecting the energy balance during plasma detachment [2, 3]. Radiation power profile measurements are key to understanding the physical mechanisms and controlling the plasma detachment.

An InfraRed Imaging Video Bolometer (IRVB) [4] has been developed for two-dimensional radiation intensity distribution measurements. To date, IRVBs have been installed at the LHD [5, 6], JT-60U [7], and KSTAR [8] to investigate the radiation intensity distribution during plasma detachment and radiation collapse phenomena. As an IRVB obtains 2D images, it can also be used to reconstruct 3D radiation intensity distributions by tomographic techniques [9].

In this study, experiments were performed using the IRVB measurement system upstream of a GAMMA 10/PDX divertor-simulated plasma in order to understand the impurity transport and energy balance in the process of plasma detachment.

2. Experimental Setup

GAMMA 10/PDX is a tandem mirror device consisting of four regions: the central cell, anchor cells, plug/barrier cells, and end regions. As shown in Fig. 1, the hydrogen plasma produced in the central cell flows into the end region through the anchor and plug/barrier cells. End-loss plasmas have high ion and electron temperatures, and can simulate scrape-off layer (SOL)-divertor plasmas.

In the west end region, a divertor simulation experimental module (D-module) was installed to investigate several phenomena in divertor plasma [10–15]. The gas-injection port was located in D-module. The number of incident neutral particles was controlled by the plenum pressure stored in the reservoir tank and the solenoid valve opening time. An IRVB was installed at the west plug-barrier cell, upstream of the divertor-simulated plasma from the D-module.

Figure 1 (b) shows a schematic of the IRVB installed in the west plug/barrier cell (Z = 920 cm, as indicated in Fig. 1 (a)). Plasma radiation was projected onto thin foil through an aperture (1 cm × 1 cm). The temperature increase in the thin foil rises corresponds to the distribution of plasma radiation. An IR camera (FLIR/Tau2, 60 fps)

author's e-mail: shigematsu_naoki@prc.tsukuba.ac.jp
*) This article is based on the presentation at the 31st International Toki Conference on Plasma and Fusion Research (ITC31).

observes the 2D temperature profile through the ZnSe window with an anti-reflection coating. The 2D image of the thin foil temperature is expressed by the following equation [16], and the plasma radiation intensity $\Omega_{\rm rad}$ is obtained;

$$-\Omega_{\rm rad} + \Omega_{\rm bb} + \frac{1}{\kappa}\frac{\partial T}{\partial t} = \frac{\partial^2 T}{\partial x^2} + \frac{\partial^2 T}{\partial y^2}, \quad (1)$$

$$\Omega_{\rm rad} = \frac{P_{\rm rad}}{kt_f} \quad \Omega_{\rm bb} = \frac{\epsilon\sigma_{\rm S\text{-}B}(T^4 - T_0^4)}{kt_f}.$$

where, κ is the thermal diffusivity of the foil; t_f is the foil thickness; k is thermal conductivity of the foil; is the emissivity; $\sigma_{\rm S\text{-}B}$ is the Stefan Boltzmann coefficient; T_0 is the background temperature; T is the 2D temperature distribution on the foil; is the blackbody radiation from the thin foil; $\Omega_{\rm bb}$ and $P_{\rm rad}$ is the plasma radiation intensity obtained by solving Eq. (1) and the results obtained using an IR camera. The distributions of thin foil parameters of κ (approximately $34.31 \pm 2.15\,{\rm mm^2/s}$), k (approximately $45.94 \pm 2.97\,{\rm W/mm/K}$), t_f and ϵ (approximately 1.04 ± 0.07) were calibrated by laser irradiation experiments and the finite element method [17]. In this experiment, the thin foil had a thickness of 1 μm; however, after coating with carbon on both sides [18], the thickness of the thin foil was calibrated at 2 μm.

Initially, a Pt foil was used for the foil detector of the IRVB, similar to the LHD [19]; however, its sensitivity was lower for GAMMA 10/PDX. Hence, a Ti foil was installed to increase sensitivity. The sensitivity of the IRVB can be expressed as the noise-equivalent power density (NEPD) [16]. NEPD improved from 280 to 90 $\mu{\rm W/cm^2}$ after replacing the Pt foil with a Ti foil [20]. The IRVB consisted of 14×18 channels in the GAMMA 10/PDX.

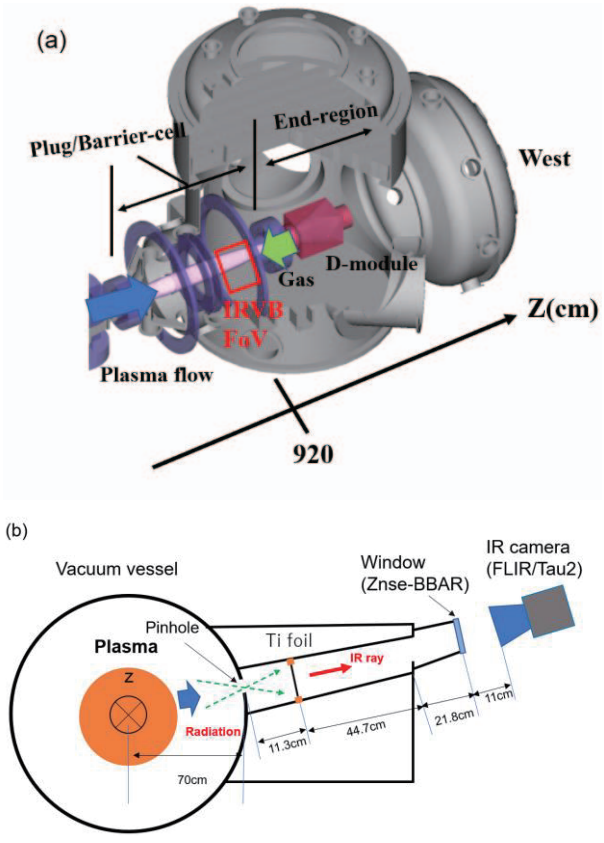

Fig. 1 Schematics of (a) west Plug/Barrier-cell and End-region and (b) IRVB of GAMMA 10/PDX.

3. Results and Discussion

Hydrogen plasma was generated by the gas puff and plasma gun at the time $t = 50$ ms and sustained by ICRF heating for 400 ms. In this experiment, plasma parameters in the central cell were as follows. The diamagnetism (DMcc) was approximately 0.35×10^{-4} Wb and the line density (NLcc) was $5.5 \times 10^{13}\,{\rm cm^{-2}}$. In this study, Ar and Ne were injected into the D-module at different plenum pressures to investigate the differences in the plasma radiation intensity profile among the gas species and injection gas pressures. Table 1 lists the shot numbers, injection gas species, and plenum pressures in the reservoir tank. Both gases were injected at the beginning of plasma discharge ($t = 50$ ms), and feeding was stopped at the end of discharge ($t = 450$ ms). The neutral gas pressure in the D-module was measured using an ASDEX gauge [11]. Figure 2 shows the time evolution of the neutral gas pressure in the D-module under each condition.

3.1 Ar gas injection

Temperature on the Ti foil in the IRVB increased by 0.1 - 0.2 K during Ar injection. Figure 3 shows the results obtained by solving Eq. (1) for distribution of the radiated

Table 1 Gas injection conditions.

Shot No.	Gas	Plenum pressure (mbar)
253930	Ar	1000
253934	Ar	800
253937	Ar	400
253941	Ne	1000
253944	Ne	800
253947	Ne	400

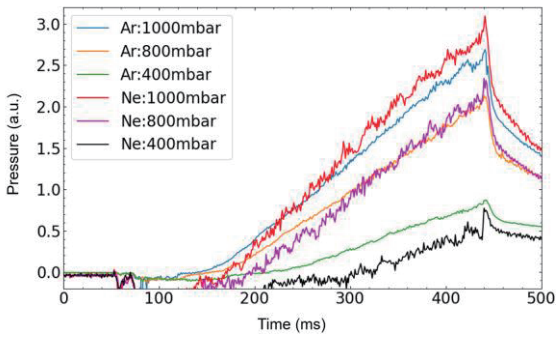

Fig. 2 Time evolution of neutral gas pressure in the D-module with ASDEX gauge.

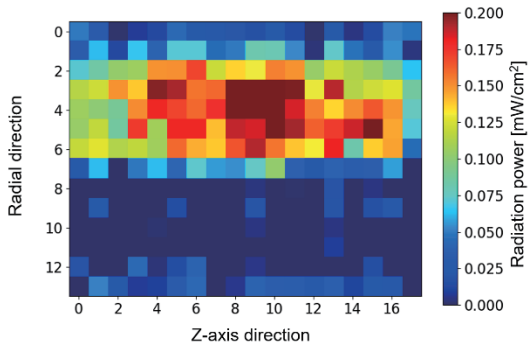

Fig. 3 Plasma radiation profile at t = 400 ms during Ar injection with plenum pressure of 1000 mbar.

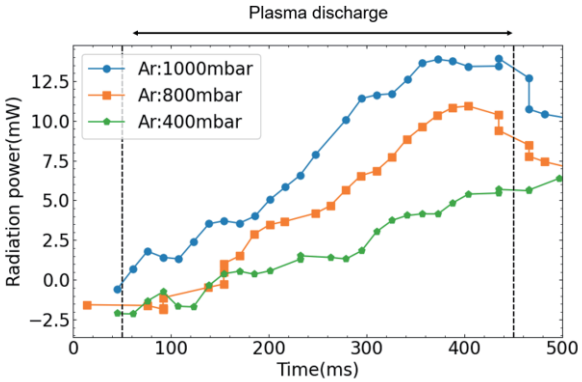

Fig. 4 Time evolution of the radiation intensity at each plenum pressure during Ar injection. Plasma discharge time is between the black dashed lines.

power absorbed by the foil at $t \cong 400$ ms for the case of that Ar plenum pressure of 1000 mbar. The plasma radiation distribution captured a zonal distribution corresponding to the magnetic-field line structure in the observed area. The plasma radiation intensity was clearly detected in seven bolometer pixels in the radial direction. Figure 4 shows the time evolution of the plasma radiation intensity integrated over the entire foil observed for each plenum pressure. The plasma radiation intensity represents the moving average. Evidently, the larger the plenum pressure, the faster the signal increased, and the larger the peak value of radiation intensity. Radiation intensities increased after plasma discharge began owing to the effect of Ar gas and decreased at the end of discharge. Note that the peak-out timing is different for each shot, and the data transfer rate most be obtained more accurately.

Next, a comparison was made between spectroscopy and soft X-ray instrumentation to investigate the validity of the time evolution of the radiation intensity obtained by the IRVB. Spectroscopic measurements were made in the visible light range (350 - 820 nm) using a spectrometer USB2000+, which was set at the west plug/barrier cell (Z = 920 cm), where is the same as the IRVB's field of view. AXUV diodes (AXUV16ELG) were used as X-ray

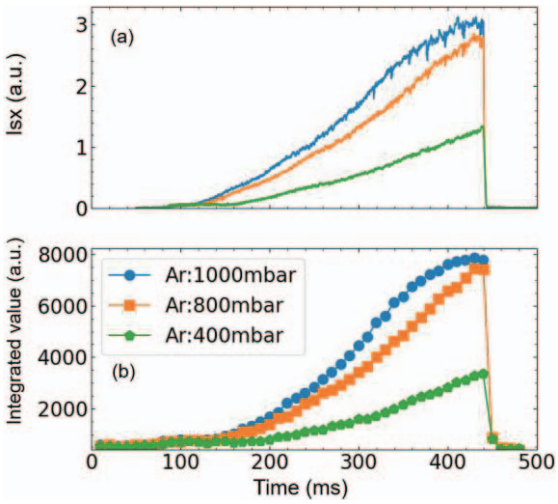

Fig. 5 (a) Time evolution of the plasma radiation in XSD measurements. (b) Time evolution of integrated values in the visible light range in USB2000+ measurements.

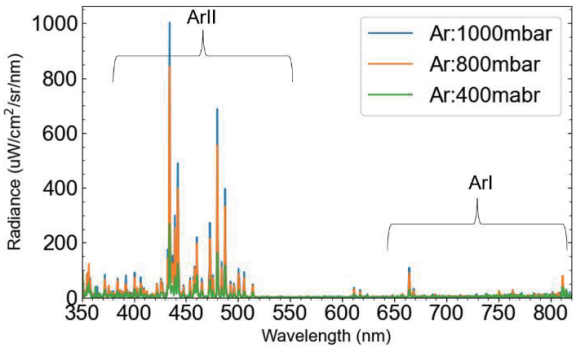

Fig. 6 Emission spectrum at t = 400 ms during Ar injection.

detectors (XSD) [21] for the soft X-ray measurements.

The XSD was placed at Z = 886 cm and had 16 channels in the radial direction to measure the radial profile of line-integrated plasma radiation. Figure 5 (a) shows the line-integrated plasma radiation intensity from the single channel closest to the center of the plasma measured using XSD. Figure 5 (b) shows the time evolution of the integrated emission intensities over the entire spectrum range of the spectrometer for comparison with the IRVB and XSD. Both measurements show that the intensity increases with increasing gas pressure. These trends are consistent with the IRVB measurements.

Figure 6 shows the spectral emission lines at t = 400 ms obtained using a USB2000+. Under all gas-injection conditions, the ArII spectral intensities were considerably higher than those of neutral Ar. A comparison with visible spectroscopy and XSD measurements suggested that the radiation intensity observed by IRVB was dominated by the emission from Ar^+ ions.

3.2 Ne gas injection

Figures 7, 8 (a), and 8(b) show the observed results for

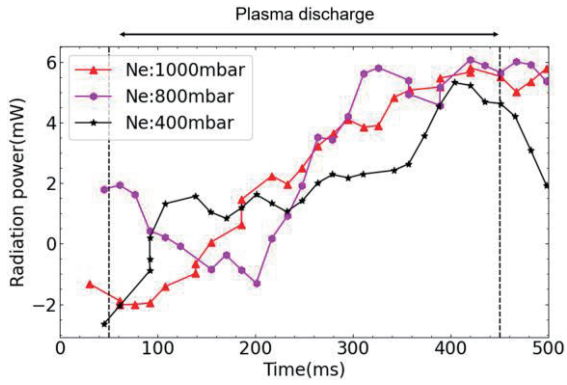

Fig. 7 Time evolution of plasma radiation during Ne injection measured by the IRVB.

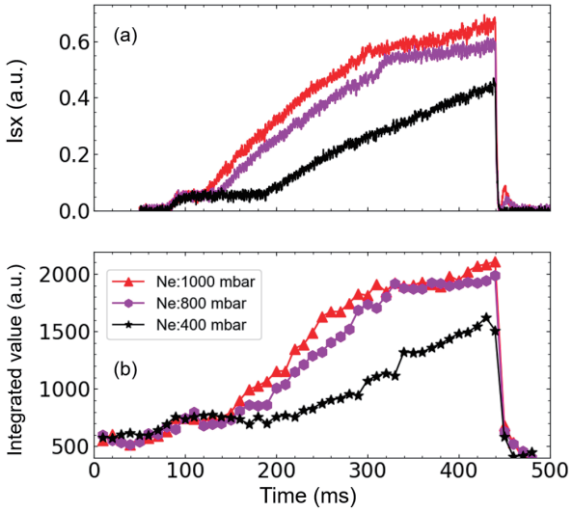

Fig. 8 In Ne injection, (a) XSD and (b) integrated values in the visible light in USB 2000+.

Ne at different plenum pressures using the IRVB (Fig. 7), XSD, and spectrometer, respectively. At low Ne pressures, the radiation intensity peaked earlier in the IRVB than at other pressures. The intensity increased with increasing pressure in the spectrum and XSD measurements, similar to the case of Ar injection. However, the IRVB measurements did not exhibit a clear effect of the radiation on the plenum pressure, unlike in the case of Ar injection. The plasma radiation intensity was consider to be weak during Ne seeding. Therefore, the IRVB signal-to-noise ratio was reduced to measure plasma radiation. The lower limit of this measurement must be further investigated. Moreover, no emission from the Ne ions was observed using the spectrometer. The first ionization energy of Ne (21.6 eV) is higher than that of Ar (15.78 eV). Generally, Ne exhibits the highest emissivity at an electron temperature of approximately 50 eV. Since our experimental electron temperature is T_e = 20 - 30 eV, the radiation emissivity of Ar was higher than that of Ne.

4. Summary

This study investigated the impurity transport and energy balance during plasma detachment. Herein, an IRVB system was developed in the west plug/barrier cells of GAMMA 10/PDX. During Ar injection, the radiation intensity increased with increasing plenum pressure. Moreover, Ar-ion emission was dominant. By contrast, no dependence between plenum pressure and radiation intensity was observed for the IRVB during Ne injection. Owing to the high first ionization energy, Ne ionization may not occur, thereby resulting in low radiation intensity.

In future studies, we will investigate the details of the impurity transport processes by comparing the plasma radiation power measured by the IRVB with the modeling results obtained using a 2D fluid simulation.

Acknowledgments

This work was partly supported by JSPS KAKENHI Grant Numbers 19K03790 and, 22H01198, and the NIFS Collaboration Research program (NIFS19KUGM137, NIFS19KUGM146, and NIFS20KUGM148). Special thanks to the GAMMA 10 group for their help with the experiments.

[1] S. Takamura *et al.*, Plasma Sources Sci. Technol. **11**, A42 (2002).
[2] N. Ezumi *et al.*, J. Nucl. Mater. **241-243**, 349 (1997).
[3] A. Kallenbach *et al.*, Plasma Phys. Control. Fusion **58**, 045013 (2016).
[4] B.J. Peterson, Rev. Sci. Instrum. **71**, 3696 (2000).
[5] K. Mukai *et al.*, Nucl. Fusion **55**, 083016(9pp) (2015).
[6] B.J. Peterson *et al.*, Nucl. Mater. Energy **26**, 100848 (2021).
[7] B.J. Peterson *et al.*, Rev. Sci. Instrum. **79**, 10E301 (2008).
[8] J. Jang *et al.*, Curr. Appl. Phys. **18**, 461 (2018).
[9] R. Sano *et al.*, Rev. Sci. Instrum. **87**, 053502 (2016).
[10] N. Ezumi *et al.*, Nucl. Fusion **59**, 066030 (2019).
[11] H. Gamo *et al.*, Plasma Fusion Res. **16**, 2402041 (2021).
[12] M. Sakamoto *et al.*, Nucl. Mater. Energy **12**, 1004 (2017).
[13] K. Nojiri *et al.*, Nucl. Mater. Energy **12**, 100691 (2019).
[14] Y. Nakashima *et al.*, Fusion. Sci. Technol. **68,** 28 (2015).
[15] Y. Nakashima *et al.*, Nucl. Fusion **57**, 116033 (2017).
[16] B.J. Peterson *et al.*, Rev. Sci. Instrum. **74**, 2040 (2003).
[17] R. Sano *et al.*, Plasma Fusion Res. **7**, 2405039 (2012).
[18] R. Sano *et al.*, Plasma Fusion Res. **6**, 2406076 (2011).
[19] K. Mukai *et al.*, Plasma Fusion Res. **9**, 3402037 (2014).
[20] K. Mukai *et al.*, Rev. Sci. Instrum. **92**, 063521 (2021).
[21] R. Minami *et al.*, Rev. Sci. Instrum. **85**, 11D807 (2014).